Novel Flyback DC-DC Converter with Improved Stability and Dynamic Response

Hiroto Terashi [1)], Isaac Cohen[2)], and Tamotsu Ninomiya[3)]

1)**Densei-Lambda KK.**, 215 Kamitakakuma-cho, Kanoya, Kagoshima, 893-0131, JAPAN
Tel.+81-994-45-2525, Fax.+81-994-45-2528, E-mail: h.terashi@densei-lambda.com
2)**Lambda Electronics Inc.**, 515 Broad Hollow Road, Melville, New York, 1174-3700, USA
Tel.+1-631-649-4200, Fax.+1-631-293-0519, E-mail: isaac.cohen@psd.invensys.com
3)**Kyushu University**, Dept. of EESE, Hakozaki, Higashi-ku ,Fukuoka, 812-8581, JAPAN
Tel.+81-92-642-3901, Fax.+81-92-642-3957, E-mail: ninomiya@ees.kyushu-u.ac.jp

Abstract

This paper proposes a novel flyback topology and its control scheme, where some disadvantages of the conventional one are eliminated while the circuit simplicity is maintained, and furthermore confirms the improvement of its dynamic response and stability analytically and experimentally.

1. Introduction

Flyback DC-DC converters are often used as power supply for many electronic systems because of the circuit simplicity. However, the conventional flyback converter has the following disadvantages: First, the frequency bandwidth of the open-loop transfer function is less than the forward converter because this transfer function has a right-half-plane zero (RHPZ). Second, a sudden decrease of output voltage called "Jumping phenomenon" appears due to internal parasitic resistances when the duty ratio becomes close to the unity.

In this paper, we propose a novel flyback topology and its control scheme, where the above disadvantages are eliminated while the circuit simplicity is maintained, and furthermore confirms the improvement of its dynamic response and stability analytically and experimentally.

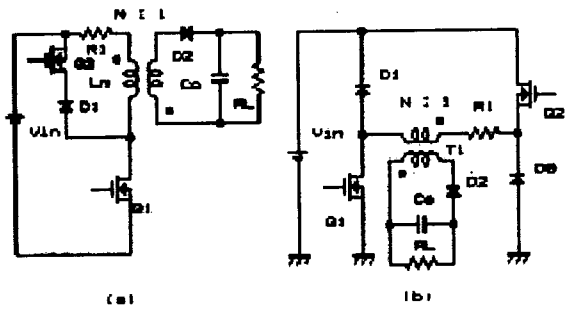

Fig 1. Novel topologies of a flyback DC-DC converter

2. Behavior of novel flyback converter

Figure 1 shows two types of a novel flyback converter, where an active current-clamp circuit is added to the conventional flyback converter. Figure 2 shows the time sequence of gate drive voltages for two switches Q1 and Q2, the magnetizing current Im of transformer, the secondary current through diode D2, and the transformer voltage.

We explain the operation of the circuit shown in Fig.1 (a) as a example of the proposed novel flyback converter.

State 1: At first, turn on both Q1 and Q2 switches. Diode D1 is reverse-biased. The input voltage Vin is applied across the primary side of the transformer. Then the diode D2 is also reverse-biased. Therefore, the energy is charged in the primary inductance Lp during the interval of DT, where the duty ratio of Q1 is denoted by symbol D and the switching period is by symbol T.

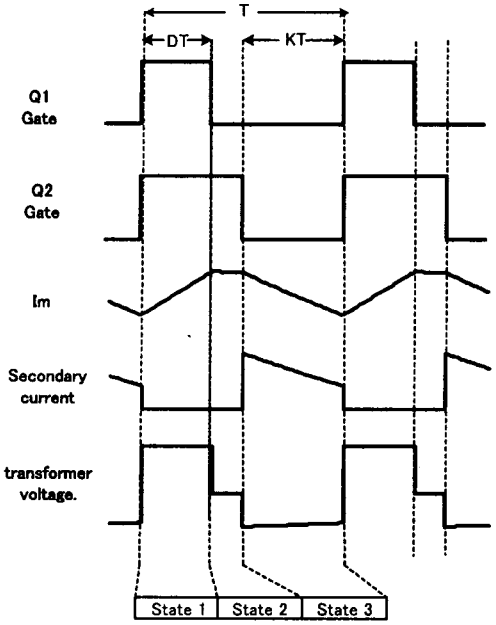

Fig 2. Key waveforms of the novel topology

State 2: When Q1 is turned off, the primary inductor current flows through the switch Q2, and the energy stored in Lp is kept to be constant.

State 3: Turn off the switch Q2. The energy stored in the transformer is transferred to the secondary side during the fixed interval of KT.

The difference between this new topology and the conventional flyback one is to insert an energy storage time of (1-D-K)T and to fix the energy discharge time of KT.

As the result, the input-to-secondary output voltage conversion ratio M becomes proportional to duty ratio D similarly to the forward converter. This relationship is easily derived from replacing the term of 1-D in the voltage conversion ratio D/(1-D) of the conventional flyback converter with the constant value of K.

3. Analysis of Dynamic characteristics

3-1. Conventional flyback converter

As seen in many literatures, the conventional flyback converter shown in Fig.3 has a 2nd-order transfer function with a right-half-plane zero (RHPZ), and a so-called jumping phenomenon appears when the duty ratio becomes larger[2]. When the load current becomes heavier and the output voltage decreases, the duty ratio is made larger for the output voltage regulation. However, the duty ratio becomes close to the unity, the output voltage jumps down to a low voltage outside the regulation range as shown in Fig.4.

The analytical expressions of steady-state and dynamic characteristics have been derived in a lot of previous literatures. The voltage conversion ratio Mc and the small-signal control-to-output transfer function Fc(s) are shown as follows:

$$M_c = \frac{D}{D' \cdot N \cdot (1 + \frac{R_1 \cdot D}{R \cdot D'^2})} \tag{1}$$

$$Fc(s) = \frac{Vin}{D'^2 \cdot N} \cdot \frac{1 - \frac{R_1 \cdot D^2}{R \cdot D'^2}}{(1 + \frac{R_1 \cdot D}{R \cdot D'^2})^2} \cdot \frac{1 - \frac{s}{\omega_Z}}{\left(\frac{s}{\omega_0}\right)^2 + 2 \cdot \varsigma_0 \cdot \frac{s}{\omega_0} + 1} \tag{2}$$

where

R1 : Parasitic resistance in primary side,

$C = Co / N^2$, $R = N^2 R_L$, $D' = 1 - D$,

$$\omega_Z = \frac{D'^2 \cdot R}{Lm \cdot D} \cdot \left(1 - \frac{R_1 \cdot D^2}{R \cdot D'^2}\right) \tag{3}$$

$$\omega_0^2 = \frac{D'^2}{Lm \cdot C} \cdot \left(1 + \frac{R_1 \cdot D}{R \cdot D'^2}\right) \tag{4}$$

$$\varsigma_0 = \frac{1}{2 \cdot \omega_0} \cdot \left(\frac{R_1 \cdot D}{Lm} + \frac{1}{C \cdot R}\right) \tag{5}$$

3-2. Novel flyback converter

This topology has three states during one switching period

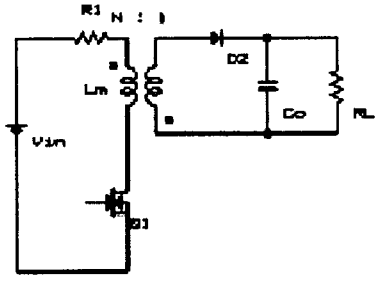

Fig 3. Conventional Flyback converter

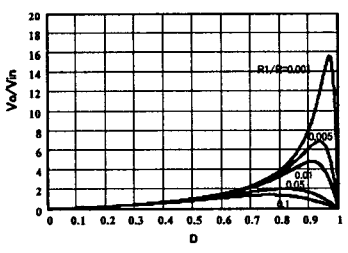

Fig 4. Control characteristics of conventional flyback converter

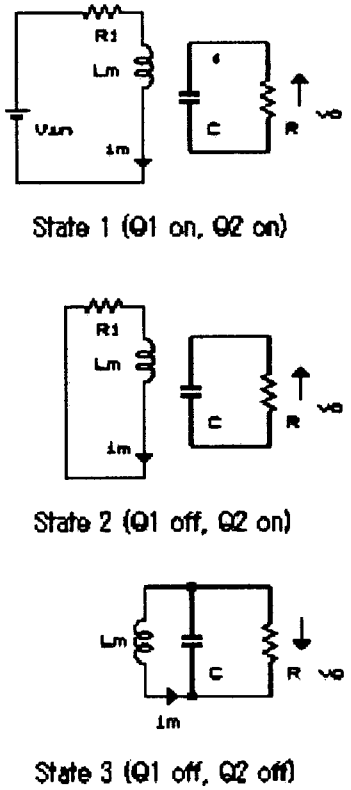

Fig 5. States of operation

as shown in Fig.5. Their durations are D for state1, (1-D-K)T for state2, and KT for state3, respectively.

The state-space equations are obtained as shown below, regarding two state variables of the magnetizing current i_m and the equivalent output voltage v_o referred to the primary side. Here, these two state variables are combined as the following vector x:

$$x = \begin{pmatrix} i_m \\ v_o \end{pmatrix}$$

State 1

$$\dot{x} = \begin{pmatrix} -\frac{R_1}{L_m} & 0 \\ 0 & -\frac{1}{C \cdot R} \end{pmatrix} \cdot x + \begin{pmatrix} \frac{1}{L_m} \\ 0 \end{pmatrix} \cdot Vin \tag{6}$$

State 2

$$\dot{x} = \begin{pmatrix} -\frac{R_1}{L_m} & 0 \\ 0 & -\frac{1}{C \cdot R} \end{pmatrix} \cdot x \tag{7}$$

State 3

$$\dot{x} = \begin{pmatrix} 0 & -\frac{1}{L_m} \\ \frac{1}{C} & -\frac{1}{C \cdot R} \end{pmatrix} \cdot x \tag{8}$$

By applying the state-space averaging method to these three states, the following differential equation is derived:

$$\dot{\hat{x}} = A \cdot \hat{x} + \begin{pmatrix} \frac{D}{L_m} \\ 0 \end{pmatrix} \cdot Vin \tag{9}$$

$$A = \begin{pmatrix} -\frac{R_1}{L_m} \cdot (1-K) & -\frac{K}{L_m} \\ \frac{K}{C} & -\frac{1}{C \cdot R} \end{pmatrix} \tag{10}$$

The steady-state characteristics are obtained by substituting $\dot{\hat{x}} = 0$ in the above equation as follows:

$$X = \frac{D \cdot Vin}{K^2 \cdot \left\{1 + \frac{R_1 \cdot (1-K)}{R \cdot K^2}\right\}} \cdot \begin{pmatrix} \frac{1}{R} \\ K \end{pmatrix} \tag{11}$$

Subsequently, using the perturbation of

$$\hat{x} = X + \Delta\hat{x}, d = D + \Delta d, vin = Vin + \Delta vin \tag{12}$$

and the linear approximation around the operating point, an equation representing the small-signal model is derived as follows:

$$\Delta\dot{\hat{x}} = A \cdot \Delta\hat{x} + \begin{pmatrix} \frac{Vin}{L_m} \\ 0 \end{pmatrix} \cdot \Delta d + \begin{pmatrix} \frac{D}{L_m} \\ 0 \end{pmatrix} \cdot \Delta vin \tag{13}$$

From this equation, the effect of duty-ratio variation on the state vector is expressed as

$$\frac{\Delta\hat{x}}{\Delta d} = \frac{Vin}{K^2 \cdot \left(1 + \frac{R_1 \cdot (1-K)}{R \cdot K^2}\right)} \frac{1}{\left(\frac{s}{\omega_1}\right)^2 + 2 \cdot \varsigma_1 \cdot \left(\frac{s}{\omega_1}\right) + 1} \cdot \begin{pmatrix} s \cdot C + \frac{1}{R} \\ K \end{pmatrix} \tag{14}$$

where

$$\omega_1^2 = \frac{K^2}{L_m \cdot C} \cdot \left(1 + \frac{R_1 \cdot (1-K)}{R \cdot K^2}\right) \tag{15}$$

$$\varsigma_1 = \frac{1}{2 \cdot \omega_1} \cdot \left(\frac{R_1 \cdot (1-K)}{L_m} + \frac{1}{C \cdot R}\right) \tag{16}$$

Therefore the voltage conversion ratio Mn and the control-to-output voltage transfer function Fn(s) are obtained as follows:

$$Mn = \frac{D}{K \cdot N \cdot \left(1 + \frac{R_1 \cdot (1-K)}{R \cdot K^2}\right)} \tag{17}$$

$$Fn(s) = \frac{Vin}{K \cdot N} \cdot \frac{1}{1 + \frac{R_1 \cdot (1-K)}{R \cdot K^2}} \cdot \frac{1}{\left(\frac{s}{\omega_1}\right)^2 + 2 \cdot \varsigma_1 \cdot \left(\frac{s}{\omega_1}\right) + 1} \tag{18}$$

As seen from (17), the voltage conversion ratio Mn is proportional to the duty ratio because K is chosen as a constant, and then the cause of the jumping phenomenon disappeared. The control-to-output voltage transfer function Fn(s) expressed by (18) has no RHPZ similarly to the forward converter. As a result, the stability and the dynamic response can be much improved when compared with the conventional flyback converter.

4. Experimental confirmation

In the experiment, the switching frequency of 300kHz was chosen to reduce the transformer size, and the magnetizing inductance Lm was set to be about 60μH. The values of other parameters were set as shown below: Input voltage Vin=48V, Output voltage Vo=5V, Turns ratio N=6, Output capacitance Co=72μF, Load resistance R_L=1Ω and K=0.5.

The frequency responses were measured by Gain-Phase Analyzer HP 4194A as shown in Figs.6 and 8.

As seen from Fig.6, the frequency response of the control-to-output transfer function Fn(s) does not have a phase lag larger than 180 degrees, and hence the transfer function Fn(s) of the proposed flyback converter has no RHPZ and has the same characteristics as the forward converter. The theoretical frequency response Fn(s) was calculated from (18), and is shown in Fig.7. They agree with a little difference of gain, and so the analysis has been experimentally confirmed.

For comparison, the frequency response Fc(s) of the conventional flyback converter has also been checked

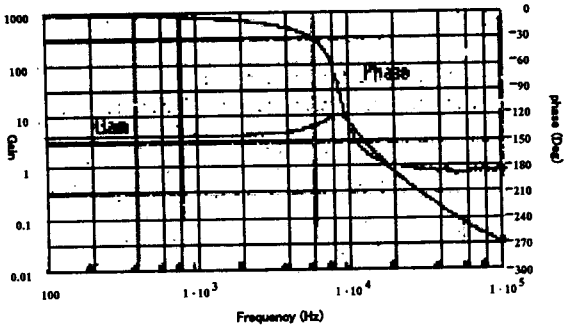

Fig 6 Measured frequency response Fn(s) of proposal converter

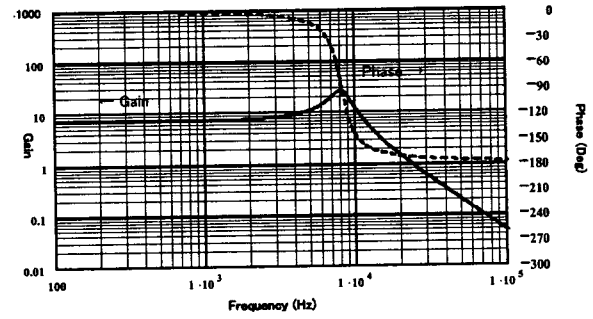

Fig 7 Thoretical frequency response Fn(s) of proposal converter

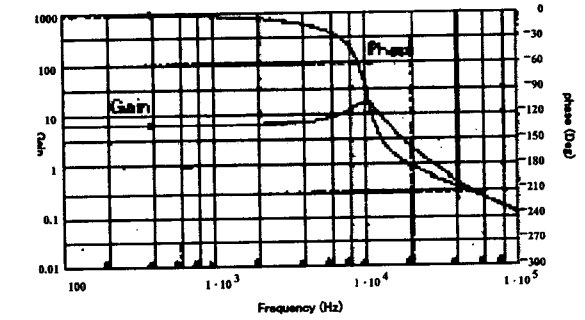

Fig 8 Measured frequency response Fc(s) of conventional coverter

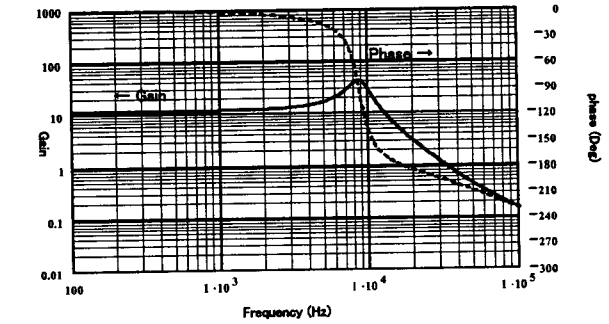

Fig.9Theoretical frequency response Fc(s) of conventional converter

theoretically and experimentally. These frequency responses are shown in Figs.8 and 9. As seen from these results, it is evident that the control-to-output transfer function of the conventional flyback converter has an RHPZ and a large phase lag

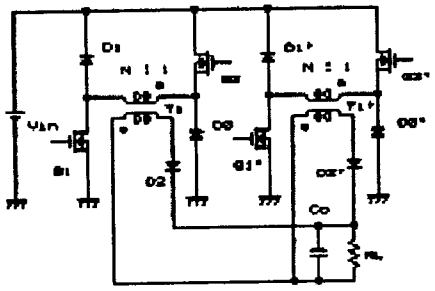

Fig 10 Application to two-phase interleaved converter

5. Application of proposed flyback converter

Recently, the power supply with low-voltage and high-current output has been required in many electronic equipments using LSIs. In this case, the application of the proposed flyback converter is effective because of the circuit simplicity. We are now investigating the interleaved topology of the proposed converters by connecting two converters in parallel and driving them in 2-phase mode alternately. Its circuit configuration is shown in Fig.10, where the topology shown in Fig.1(b) is utilized. The merit of this configuration is that the frequency components of input and output currents are twice of the switching frequency and therefore the voltage ripples are made much smaller than a single-converter configuration. The converter system with the output condition of 3.3V and 50A is now under investigation.

6. Conclusion

A novel flyback converter and its control scheme have been proposed. By adding only one auxiliary switch to the conventional flyback converter and fixing the discharging interval of the energy stored in the transformer, the input-to-output voltage conversion ratio becomes proportional to the duty ratio, and the RHPZ disappears from the control-to-output transfer function. Consequently, the dynamic characteristics can be much improved.

The analysis and the experimental confirmation have clarified the improvement of the stability and dynamic response of this modified flyback converter.

Furthermore, the extension of this proposed converter to the practical application has been considered.

Reference

[1] T.Ninomiya, M.Nakahara, T.Higashi, K.Harada: "A Unified Analysis of Resonant Converters," IEEE Trans. on Power Electronics, Vol.PE-6, No.2, April 1991, pp. 260-270.

[2] T.Ninomiya, K.Harada, M.Nakahara "Stability Analysis of Boost and Buck-Boost Converters," The Trans. of IEIEC, Vol.J66-C, No.1, Jan. 1983, pp.1-8.